Factors controlling tropospheric O_3, OH, NO_x, and SO_2 over the tropical Pacific during PEM-Tropics B

Yuhang Wang,[1] Shaw C. Liu,[2,3] Paul H. Wine,[2,4] Douglas D. Davis,[2] Scott T. Sandholm,[2] Eillot L. Atlas,[5] Melody A. Avery,[6] Donald R. Blake,[7] Nicola J. Blake,[7] William H. Brune,[8] Brian G. Heikes,[9] Glen W. Sachse,[6] Richard E. Shetter,[5] Hanwant B. Singh,[10] Robert W. Talbot,[11] and David Tan[8,12]

Abstract. Observations over the tropical Pacific during the Pacific Exploratory Mission (PEM)-Tropics B experiment (March-April 1999) are analyzed. Concentrations of CO and long-lived nonmethane hydrocarbons in the region are significantly enhanced due to transport of pollutants from northern industrial continents. This pollutant import also enhances moderately O_3 concentrations but not NO_x concentrations. It therefore tends to depress OH concentrations over the tropical Pacific. These effects contrast to the large enhancements of O_3 and NO_x concentrations and the moderate increase of OH concentrations due to biomass burning outflow during the PEM-Tropics A experiment (September-October 1996). Observed CH_3I concentrations, as in PEM-Tropics A, indicate that convective mass outflux in the middle and upper troposphere is largely independent of altitude over the tropical Pacific. Constraining a one-dimensional model with CH_3I observations yields a 10-day timescale for convective turnover of the free troposphere, a factor of 2 faster than during PEM-Tropics A. Model simulated HO_2, CH_2O, H_2O_2, and CH_3OOH concentrations are generally in agreement with observations. However, simulated OH concentrations are lower (~25%) than observations above 6 km. Whereas models tend to overestimate previous field measurements, simulated HNO_3 concentrations during PEM-Tropics B are too low (a factor of 2-4 below 6 km) compared to observations. Budget analyses indicate that chemical production of O_3 accounts for only 50% of chemical loss; significant transport of O_3 into the region appears to take place within the tropics. Convective transport of CH_3OOH enhances the production of HO_x and O_3 in the upper troposphere, but this effect is offset by HO_x loss due to the scavenging of H_2O_2. Convective transport and scavenging of reactive nitrogen species imply a necessary source of 0.4-1 Tg yr^{-1} of NO_x in the free troposphere (above 4 km) over the tropics. A large fraction of the source could be from marine lightning. Oxidation of DMS transported by convection from the boundary layer could explain the observed free tropospheric SO_2 concentrations over the tropical Pacific. This source of DMS due to convection, however, would imply in the model free tropospheric concentrations much higher than observed. The model overestimate cannot be reconciled using recent kinetics measurements of the DMS-OH adduct reaction at low pressures and temperatures and may reflect enhanced OH oxidation of DMS during convection.

1. Introduction

The Pacific Exploratory Mission (PEM) - Tropics B experiment took place during March-April 1999 [*Raper et al.*, this issue]. The mission was conducted using two aircraft, DC-8 and P-3B. Flights of the DC-8 surveyed areas around Hawaii, Fiji, Tahiti, and Easter Island from the boundary layer up to 12-km altitude, whereas the P-3B flights with an emphasis on sampling the tropical lower troposphere surveyed below 6 km mostly between Hawaii and Tahiti. Previously, the PEM-Tropics A experiment sampled similar regions over the tropical Pacific in September-October 1996 [*Hoell et al.*, 1999]. One prominent feature observed during PEM-Tropics A was the prevalent influence of biomass burning plumes over the tropical Pacific [*Blake et al.*, 1999; *Schultz et al.*, 1999; *Talbot et al.*, 1999]. *Wang et al.* [2000] analyzed the effects of biomass burning outflow using a one-dimensional (1-D) model. Observations in the tropics were binned into three equally divided groups (tertiles) by C_2H_2 concentrations. The upper tertile data

group showed clear chemical signatures of biomass burning outflow with high concentrations of O_3, NO_x ($NO+NO_2$), and CO, whereas the lower tertile group was much cleaner with low concentrations of pollutants. The PEM-Tropics B experiment sampled over the tropical Pacific in March-April, when biomass burning is not expected to be significant in the tropics. Nevertheless, high-concentration pollutant plumes were encountered [*Blake et al.*, this issue]. We will compare the chemical signatures observed during the two PEM-Tropics missions in different seasons and examine the likely sources of the pollutant inflow into the tropical Pacific and their effects. We will examine, in particular, the effects of pollutants on tropical OH concentrations, which constitute a substantial portion of the oxidizing power of the atmosphere [Intergovernmental Panel on Climate Change (*IPCC*), 1996].

Convection can have profound impact on chemistry in the tropics. One aspect examined by *Prather and Jacob* [1997] is the HO_x ($OH+HO_2$) source enhancement in the upper troposphere due to photolysis of CH_3OOH transported convectively from the lower troposphere. *Müller and Brasseur* [1999] estimated that this source dominates other primary HO_x sources in the tropical upper troposphere. During PEM-Tropics A, *Wang et al.* [2000] found that its effects on O_3 and OH concentrations are generally too small to compare with those of biomass burning outflow. The PEM-Tropics B experiment, which sampled air much cleaner than that in PEM-Tropics A, offers a better opportunity to examine this and other aspects of the effects on tropical trace gas composition by convection. Furthermore, four key species (OH, HO_2, CH_2O, and acetone), not measured during PEM-Tropics A, were measured during PEM-Tropics B and can be used to better constrain HO_x chemistry.

In addition to the O_3-HO_x-NO_x chemistry over the tropical Pacific, examined by *Wang et al.* [2000] for PEM-Tropics A, we will investigate sources of SO_2 in the free troposphere. *Thornton et al.* [1999] reviewed 1991-1996 aircraft SO_2 measurements over the Pacific. They suggested that anthropogenic activities along the North Pacific rim and volcanic sources along the western Pacific rim contribute significantly to free-troposphere SO_2 concentrations. The contribution from DMS, emitted by oceans, appears to dominate in the boundary layer. Quantifying the link between oceanic DMS and free troposphere SO_2 is, however, important because of the implications on climate feedback [*Charlson et al.*, 1987]. We will investigate how much free-troposphere SO_2 during PEM-Tropics B may be attributed to DMS oxidation. The widely adopted rate constants for the DMS-OH adduct reaction by *Hynes et al.* [1986] were derived from experiments conducted for atmospheric conditions near surface. We will derive rate constants more appropriate for free tropospheric conditions on the basis of recent low-temperature and low-pressure measurements by *Hynes et al.* [1995] and *Barone et al.* [1996].

We will analyze observations of 15°S-15°N from the DC-8 flights to understand chemistry over the tropical Pacific; a large number of industrial plumes observed north of 15°N are therefore excluded. During the return flights from Easter Island to NASA Dryden Flight Research Center, highly polluted continental outflow was sampled. We excluded these last two flights from our analysis. Instruments used on board DC-8

are described by perspective investigators in this issue. We will take into account instrument sensitivities in our analysis. We describe in section 2 the 1-D model applied in the analysis. In section 3, we compare the chemical characteristics between PEM-Tropics A and B and examine the effects of long-range transport of pollutants over the tropical Pacific. In section 4, we analyze using the 1-D model the convective turnover timescale constrained by CH_3I observations and the impact of convection on O_3, HO_x, NO_x, DMS, and SO_2 concentrations. Conclusions are given in section 5.

2. One-Dimensional Model

Concentrations of chemical species often change rapidly with altitude. This rapid change reflects in part the changing photochemical environment with altitude and in part the relatively slow transport in the vertical compared with that in the horizontal. The vertical distribution of chemical species often provides a sensitive test for our understanding of chemistry and transport. A 1-D model is suited for such analysis. The 1-D model used in this work is described by *Wang et al.* [2000]. It is based on the model by *Trainer et al.* [1987, 1991] and *McKeen et al.* [1997]. The vertical transport of the model was originally computed using a diffusion scheme, in which the rate of tracer transport depends on the diffusion coefficient K_z and the vertical gradient of the tracer [e.g., *Liu et al.*, 1984]. The diffusion scheme alone, however, cannot represent vertical mixing of the tropospheric column in the tropics [*Wang et al.*, 2000], where convection dominates. During convection, air in the lower troposphere is lifted by updrafts into the free troposphere and air in the free troposphere is brought by subsidence to the lower troposphere. This direction-oriented transport differs from the underlying assumption of random motions in all directions in diffusion transport. *Wang et al.* [2000] implemented an explicit scheme of convective transport using specified convective mass fluxes. A diffusion coefficient is specified in the model to reproduce the observed vertical gradient of CH_3I concentrations below 2 km (section 4). Soluble species H_2O_2 and HNO_3 are scavenged during convective transport [*Wang et al.*, 2000].

The model extends to 16 km with decreasing vertical resolutions from 10 m near the surface to 1 km at the ceiling of the DC-8 aircraft (12-km altitude). The time step for transport and chemistry is 30 s. The model is run for 60 days to obtain steady state results. The kinetics data are taken from *DeMore et al.* [1997] and *Atkinson et al.* [1997], with updates from *Sander et al.* [2000]. The rate constants for the DMS-OH adduct reaction are uncertain, particularly for free tropospheric conditions [*DeMore et al.*, 1997]. We derive new rate constants from more recent kinetics measurements by *Hynes et al.* [1995] and *Barone et al.* [1996] and compare those to the widely adopted rate constants from *Hynes et al.* [1986] in section 4.4. We did not include hydrolysis of N_2O_5 on aerosols due in part to the uncertainties in the calculation of aerosol surface areas [*Schultz et al.*, 2000]; its implications on the budget of NO_x in the model are discussed in section 4.3. The total ozone column is specified to 262 Dobson Unit (DU), the average observed by the Total Ozone Mapping Spectrometer during PEM-Tropics B. The oceanic surface albedo is specified to

0.1. Model calculated photolysis rates of $J(O^1D)$ and $J(NO_2)$ agree within ±15% to the observed medians (binned in 1-km intervals) for solar zenith angle <50°, when the value of $J(NO_2)$ is insensitive to solar zenith angle. Soluble species HNO_3 and H_2O_2 deposit to water at 1 cm s^{-1} [*Wang et al.*, 1998a]. We constrain the model using observed median profiles of O_3, NO, CO, and hydrocarbons up to 12-km altitude. Concentrations of these species above 12 km are specified as the medians at 11-12 km. Concentrations of H_2O decrease with temperature to 6 ppmv at 16 km.

3. Pollutant Import: PEM-Tropics B Versus PEM-Tropics A

3.1. Sources of Pollutant Inflow

The Pacific Ocean covers more than one third of the Earth's surface. Its vast size allows long-term evolution of pollutant outflow from the continents without too much interference from fresh emissions. During PEM-Tropics A in austral spring, chemistry over the southern tropical Pacific was strongly perturbed by pollutants from biomass burning [*Blake et al.*, 1999; *Schultz et al.*, 1999; *Talbot et al.*, 1999; *Wang et al.*, 2000]. Using C_2H_2 as a tracer, *Wang et al.* [2000] estimated that biomass burning outflow enhances O_3 concentrations, O_3 production, and concentrations of NO_x and OH by 60, 45, 75, and 7%, respectively.

Air masses with enhanced concentrations of C_2H_2 were also observed during PEM-Tropics B in austral fall [*Blake et al.*, this issue]. However, this enhancement shows distinctively different chemical characteristics from those of PEM-Tropics A indicating a different origin from biomass burning. Figure 1 compares the correlation of C_2H_2 and C_2Cl_4 at 15°S-15°N between PEM-Tropics A and B. Tetrachloroethene is emitted from dry cleaning and industrial usage [*McCulloch and Midgley*, 1996] and is therefore a good industrial tracer. Its chemical lifetime is ~3 months in the tropics. Acetylene is emitted from either fossil fuel combustion and industry or biomass burning and has a lifetime of a few weeks in the tropics. Figure 1 shows a positive C_2H_2-C_2Cl_4 correlation during PEM-Tropics B, implying that C_2H_2 originated from northern industrialized continents. The scattering in the data reflects the difference in the production processes of C_2H_2 and C_2Cl_4. Their industrial origin is further supported by decreasing concentrations of C_2H_2 and C_2Cl_4 as well as CO, C_2H_6, and C_3H_8 with latitude from north to south [*Blake et al.*, this issue]. In contrast, C_2H_2 concentrations in the northern tropics were close to background levels and much lower than in the southern tropics during PEM-Tropics A [*Wang et al.*, 2000]. Furthermore, concentrations of C_2H_2 were mostly independent of comparatively low C_2Cl_4 concentrations during PEM-Tropics A, consistent with a biomass burning origin of C_2H_2 in austral spring.

Figure 1

We use C_2H_2 as a tracer for industrial pollutant outflow and group PEM-Tropics B observations into three equally divided tertiles to analyze further air chemical characteristics in the region. Figure 2 shows the vertical profiles of median concentrations of C_2H_2, CO, acetone, O_3, OH, and NO for the lower, middle, and upper tertiles of C_2H_2. The median concentrations of C_2H_2 in the lower tertile are only ~10 pptv, about factors of

Figure 2

2 and 4 lower than medians in the middle and upper tertiles, respectively. Concentrations of CO show a similar trend. The median concentrations of CO in the lower tertile of C_2H_2 is ~45 ppbv, only a few ppbv above the background CO concentration of 40 ppbv from CH_4 oxidation. Median CO concentrations in the middle and upper tertiles of C_2H_2 are significantly higher than the 40-ppbv level expected from CH_4 oxidation. The grouping of observations by C_2H_2 concentrations therefore separates air masses strongly influenced by pollutant outflow from those relatively clean and can be used to estimate the impact of pollutant outflow. The concentrations of CO and C_2H_2 exhibit generally decreasing concentrations with altitude, which was not observed during PEM-Tropics A [*Wang et al.*, 2000], implying that the lower troposphere is an important conduit for the long-range transport of northern industrial plumes but not for southern biomass burning plumes.

The median concentrations of acetone are moderately higher in higher tertiles of C_2H_2 (Figure 2) reflecting in part production of acetone from oxidation of anthropogenic hydrocarbons such as propane, the concentrations of which correlate well with C_2H_2 [*Blake et al.*, this issue]. However, the observed enhancements of 0-200 pptv due to pollutant import over a background of 400 pptv are marginal considering that standard deviations are ~100 pptv (not shown). These measurements suggest that the sources of acetone are located largely in the tropical region, most likely of biogenic origin [*Singh et al.*, 1994, 2001; *Wang et al.*, 1998b].

3.2. Timescale of Transport and Its Effects on Tropical OH Concentrations

During PEM-Tropics A, biomass burning outflow was observed to enhance significantly not only reduced compounds like C_2H_2 and CO but also O_3 and NO concentrations; model simulations indicated that it also enhanced tropical OH concentrations [*Wang et al.*, 2000] (OH was not measured on the DC-8 during PEM-Tropics A). Despite of the large enhancements in C_2H_2 and CO concentrations due to outflow from northern industrial continents, PEM-Tropics B observations (Figure 2) show only some enhancements in O_3 concentrations from lower to higher tertiles of C_2H_2. In contrast to PEM-Tropics A, concentrations of NO and OH during PEM-Tropics B were higher in the lower tertiles of C_2H_2, which represent air masses not strongly influenced by pollutant outflow.

We examine this comparison quantitatively in Table 1 by listing median column concentrations of observed O_3 and OH, as well as model computed column production of O_3, and concentrations of NO_x ($NO+NO_2$), NO_t ($NO_x + 2xN_2O_5 + HNO_4 + PAN + HNO_3$), and daytime and 24-hour average OH. The corresponding values for PEM-Tropics A are given in parenthesis. Column production and concentrations of O_3 and column NO_x more than doubled from the lower to upper tertile of C_2H_2 during PEM-Tropics A. In comparison, there is only a small increase in tropospheric O_3 column and actually a 15% decrease in O_3 production during PEM-Tropics B. The O_3 production decrease is closely related to that of NO_x (30%). The former decrease is smaller in part because column integrated O_3 production is weighted by mass favoring lower and middle troposphere, where the decrease of NO_x is not as much as in

Table 1

the upper troposphere (Figure 2).

Fresh pollutant outflow from northern industrial continents is enriched in CO, hydrocarbons, and NO_x as the biomass burning outflow. We believe that the drastically different effects on the air chemical composition over the tropical Pacific by pollutant outflow during PEM-Tropics A and B reflects a much longer timescale of transport from northern industrial continents than that of biomass burning outflow. Short-lived NO_x is depleted in the long-range transport during PEM-Tropics B but longer-lived NO_t, CO, and C_2H_2 are not. During PEM-Tropics A, on the other hand, the timescale of transport of biomass burning outflow is short enough that NO_x concentrations were also enriched. Quantitative assessments of transport timescales from available observations require a more rigorous treatment that we will undertake in a subsequent study. We will suggest in section 4.3 that NO_x observed during PEM-Tropics B is mainly from lightning.

Concentrations of OH in general depend strongly on concentrations of NO_x, CO, and hydrocarbons. Higher NO_x concentrations shift HO_2 towards OH and tend to increase OH concentrations. Carbon monoxide and hydrocarbons have the opposite effects. *Davis et al.* [this issue] examined the distributions of OH and its precursors in detail. We examine here the effects of pollutant transport on OH concentrations. During PEM-Tropics B the longer transport timescale for pollutants from northern industrial continents leaves only the imprints of long-lived CO and hydrocarbons but not so much in short-lived NO_x concentrations. The net effect is a significant decrease of observed OH concentrations from lower to upper tertiles of C_2H_2 during PEM-Tropics B (Table 1), suggesting that the long-range transport of pollutants depressed tropical OH concentrations (particularly in the southern tropics). Model results show a similar trend but simulated column concentrations are 15% lower than observations. The underestimate is due to that in the upper troposphere (section 4.2). Concentrations of OH were not measured during PEM-Tropics A; we use model results here. Table 1 shows a small increase of 7% from the lower to upper tertile of C_2H_2. The shorter transport timescale during PEM-Tropics A allowed concurrent increases of short-lived NO_x with longer-lived CO and hydrocarbons in air masses influenced by biomass burning outflow. These two factors have offsetting effects resulting in a small enhancement of OH concentrations.

4. Convective Transport and Its Effects on Photochemistry

4.1. Convective Turnover Timescale

A good chemical tracer for convection over the tropical ocean is CH_3I [*Davis et al.*, 1996; *Cohan et al.*, 1999; *Wang et al.*, 2000]. Emitted from the ocean, CH_3I has a short lifetime of ~3 days against photolysis in the tropics. The observed vertical profile of CH_3I in the free troposphere reflects a balance between the supply by convective transport and the loss by photolysis and offers good constraints on the rate of convective transport from the boundary layer into the free troposphere. *Wang et al.* [2000] analyzed the vertical distribution of CH_3I during PEM-Tropics A using the 1-D model (section 2).

Two findings are noteworthy in light of the observations from PEM-Tropics B.

Wang et al. [2000] adopted convective mass fluxes from a general circulation model (GCM), which has strong outflux in the upper troposphere but little in the middle troposphere. The 1-D simulation of CH_3I using the GCM convective statistics shows a C-shaped profile with higher concentrations in boundary layer (due to emission) and in the upper troposphere (due to convective transport). Observations of CH_3I during PEM-Tropics A, in comparison, show little altitude dependence in the free troposphere, suggesting that oceanic convective outflux distributes evenly with altitude. Figure 3 shows the median profile of CH_3I observed during PEM-Tropics B. Observed CH_3I concentrations again show little altitude dependence in the free troposphere corroborating with our finding from PEM-Tropics A.

Figure 3

We estimated a 20-day turnover timescale during PEM-Tropics A on the basis of observed CH_3I observations. Figure 3 shows that the diffusion transport (K_z = 10 m s^{-1}, the same as for PEM-Tropics A) alone captures the vertical gradient in the boundary layer but grossly underestimates CH_3I concentrations in the free troposphere. The mass fluxes adjusted to simulate PEM-Tropics A observations lead to large underestimates of CH_3I concentrations in the free troposphere. A doubling of the mass fluxes is necessary to explain PEM-Tropics B CH_3I observations. It implies a 10-day turnover timescale of the free troposphere due to convection during PEM-Tropics B.

With rapid turnover by convection and away from fresh pollutant outflow (section 3), PEM-Tropics B observations promise a good case for studying the effects of convective transport on air chemistry over the tropical Pacific. The 1-D model is constrained by observed median concentrations of O_3, NO, CO, hydrocarbons, and boundary layer DMS and SO_2. We compare with observations model simulations of OH, HO_2, CH_2O, peroxides, HNO_3, PAN, DMS, and SO_2 concentrations. The discrepancies between model and observations found in section 4.2 (hydrogen oxides and O_3) are largely independent of the C_2H_2 tertiles, as are the concentrations of free tropospheric DMS and SO_2 in section 4.4. We show therefore the model comparison with observed medians. Only in section 4.3 (nitrogen oxides) do we compare model results with observations for the three tertiles of C_2H_2 separately because observed HNO_3 and PAN concentrations vary with C_2H_2 tertiles.

4.2. Hydrogen Oxides and O_3

Hydroxyl radicals are the key species for the oxidation of reduced compounds such as CO and hydrocarbons in the troposphere [*IPCC*, 1996]. During oxidation, OH is converted to HO_2, which is recycled back to OH by reacting with NO. A key intermediate product of hydrocarbon oxidation is CH_2O. The lifetime of CH_2O is relatively short (5-10 hours) in the tropics. Its concentration therefore serves as a good gauge for photochemical activities. However, previously large discrepancies have been found between model simulated and observed CH_2O concentrations [e.g., *Fried et al.*, 1997].

Figure 4 compares simulated daytime OH, HO_2 and CH_2O

Figure 4

concentrations with observations. The model is well within the range of observed HO_2 concentrations, but underestimates OH concentrations by ~25% above 6 km. Similar results were found in point model calculations [*Olson et al.*, this issue; *Tan et al.*, this issue; J. M. Rodriguez et al., manuscript in preparation, 2001]. The discrepancy is within the instrument uncertainty of ±40% [*Faloona et al.*, 2000]; the reason for the altitude dependence of the bias is unclear.

Most of CH_2O is produced from CH_4 oxidation during PEM-Tropics B. A substantial fraction of data points are below the limit of detection (LOD) of 50 pptv. The LOD fraction increases from 30% at 7 km to 50% at 12 km (Figure 5). When the LOD fraction is >30%, we show only the median values. When the LOD fraction is >50% at 9-10 km, we use the LOD limit of 50 pptv for the median of the data bin, which is an upper limit. Model simulated CH_2O concentrations generally agree with observations but with a consistent high bias of ~25 pptv. The agreement between the model and observations are substantially better than previous missions [e.g., *Fried et al.*, 1997]. Although the lifetime of CH_2O is only a few hours, model results indicate that convection decreases CH_2O concentrations by 10-30 pptv in the lower troposphere and increases CH_2O concentrations by similar amounts in the upper troposphere. Inclusion of convection improves model comparison with observed CH_2O concentrations in the lower and middle troposphere.

Figure 5

During PEM-Tropics A, OH, HO_2, and CH_2O were not measured. Model simulations of HO_x were constrained by its longer-lived reservoirs, H_2O_2 and CH_3OOH. *Wang et al.* [2000] showed that model simulated H_2O_2 and CH_3OOH concentrations agree well with observations except some underestimates in the lower troposphere for the upper tertile of C_2H_2, associated with dry and polluted air. Figure 6 illustrates these comparisons for PEM-Tropics B and shows reasonable agreement between the model and observations for H_2O_2 concentrations but a consistent overestimate of 100-200 pptv for CH_3OOH concentrations. Including convective transport improves both simulations. The observed 3-km H_2O_2 maximum and a large drop of CH_3OOH concentrations at 0-1 km compared to higher altitudes are inconsistent with the observations of PEM-Tropics A [*Wang et al.*, 2000], which may reflect the uncertainties of ±30% in the measurements [*Hoell et al.*, 1999].

Figure 6

Convective transport of CH_3OOH into the upper troposphere boosts the production of HO_x in the region [*Prather and Jacob*, 1997]. Figure 7 shows simulated primary HO_x sources. Compared to a similar figure by *Wang et al.* [2000] for PEM-Tropics A, the crossover point at which photolysis of CH_3OOH from convective transport begins to dominate moves down from 11 km during PEM-Tropics A to 10 km due to the faster convective turnover during PEM-Tropics B. Model results suggest an enhancement of H_2O_2 concentrations above 13 km despite convective scavenging of H_2O_2 as a result of increased primary HO_x production from photolysis of convected CH_3OOH (Figure 6). Convective transport also more than doubles upper tropospheric CH_3OOH concentrations in the model.

Figure 7

This boost to the primary HO_x source from convective transport of CH_3OOH is offset by the scavenging loss of

H_2O_2, a reservoir of HO_x radicals. The latter factor dominates in the middle atmosphere. Both OH and HO_2 concentrations are lower below 9 km with convection, as are the production rates of HO_x and O_3 (Figure 8). The effects of convection on the production of O_3 should be considered over the whole tropospheric column since the convective turnover timescale of 10 days is shorter than the lifetime of O_3 above 4 km [*Wang et al.*, 2000]. Column (0-16 km) O_3 production (1.3 $x10^{11}$ molecules cm^{-2} s^{-1}) is 4% more, but column HO_x production ($6.2x10^{11}$ molecules cm^{-2} s^{-1}) and OH concentration ($1.1x10^6$ molecules cm^{-3}) are 7 and 4% less, respectively, in the convective than nonconvective case. These results obviously depend on our assumptions of convective mass fluxes and species concentrations above 12 km, which could not be constrained due to the lack of observations. They nonetheless imply relatively small effects by convection on column O_3 and OH concentrations due to the offsetting effects of convective transport of CH_3OOH and scavenging of H_2O_2. One convective effect not taking into account here is the convective transport of H_2O, which is reflected in the observed H_2O concentrations. Its effect on the HO_x primary sources is unlikely to be significant above 12 km due to the large contribution by convectively transported CH_3OOH. However, convective transport of H_2O and subsequent moistening of the atmosphere could substantially boost the primary HO_x production in the middle and lower troposphere because of the dominance of the $O(^1D)+H_2O$ reaction (Figure 7). Our model, however, is inadequate to assess this effect.

Figure 8

Figure 9 shows model diagnosed median O_3 production and loss rates and a deficit in the O_3 budget. Column O_3 production at 0-16 km is $1.3x10^{11}$ molecules cm^{-2} s^{-1} only ~50% of the column loss ($2.5x10^{11}$ molecules cm^{-2} s^{-1}) during PEM-Tropics B. Previous O_3 budget studies over the tropical Pacific also showed large deficits during PEM-West A [*Davis et al.*, 1996], PEM-West B [*Crawford et al.*, 1997], and PEM-Tropics A [*Schultz et al.*, 1999; *Wang et al.*, 2000]. The ubiquitous O_3 budget deficit over the tropical Pacific is not unexpected since the region is away from major sources of O_3 precursors. The lifetime of O_3 is long above 5 km (> 3 months) [*Wang et al.*, 2000]. Long-range transport from continents, where emissions of O_3 precursors are abundant, can make up for the column budget deficit [*Schultz et al.*, 1999; *Wang et al.*, 2000; *Browell et al.*, this issue]. Direct transport of large amounts of O_3 from the stratosphere in the tropics is unlikely [*Holton et al.*, 1995]. Additional observations are required to quantify contributions from different O_3 transport pathways. The comparisons between PEM-Tropics A and B in Table 1 offer some hints worth mentioning. Concentrations of O_3 and NO_x are similar among C_2H_2 tertiles during PEM-Tropics B despite large differences in CO and long-lived hydrocarbon concentrations (Figure 2). They are also close to the values in the lower tertile during PEM-Tropics A. These similarities imply that the sources and transport of O_3 and NO_x are largely located within the tropics, a feature simulated in a global 3-D model [*Wang et al.*, 1998c].

Figure 9

4.3. Nitrogen Oxides

Model simulations of HNO_3 concentrations generally over-

estimate field measurements [e.g., *Chatfield*, 1994; *Fan et al.*, 1994; *Jacob et al.*, 1996; *Wang et al.*, 1998b; *Lawrence and Crutzen*, 1998; *Hauglustaine et al.*, 1998]. During PEM-Tropics A, however, good agreement was obtained for the lower and middle tertiles of C_2H_2 with some model overestimates in the upper tertile of C_2H_2 [*Wang et al.*, 2000]. Figure 10 compares simulated and observed HNO_3 for the three tertiles of C_2H_2 for PEM-Tropics B. Unlike in the previous cases, simulated HNO_3 concentrations are much lower (by a factor of 2 or more) than the observed medians. Median concentrations of HNO_3 measured on the P-3B using the same type of instrument [*Talbot et al.*, 1999] are generally lower than those on the DC-8 but are still higher than model simulations. Furthermore, observed HNO_3 concentrations increase from the lower to upper tertile of C_2H_2 but simulated HNO_3 has an opposite trend because of NO_x and OH concentrations are lower in the upper tertile (Table 1, Figure 2). An obvious possibility is the hydrolysis of N_2O_5 in aerosols, not simulated in the model. However, aerosol observations do not show a discernible trend in surface area from the lower to upper tertile of C_2H_2. Aerosol NH_4^+ and SO_4^{-2} concentrations during PEM-Tropics B are also similar to PEM-Tropics A (J. Dibb, personal communication, 2000), when hydrolysis of N_2O_5 was not necessary to explain the observed HNO_3 concentrations [*Schultz et al.*, 2000; *Wang et al.*, 2000].

Figure 10

Model comparison with observations for PAN (Figure 11) shows similar results to those by *Wang et al.* [2000] for PEM-Tropics A. The model generally reproduces PAN concentrations in the lower and middle tertiles of C_2H_2, but underestimates the concentrations in the upper tertile of C_2H_2, implying long-range transport of PAN into the region. The concentrations of PAN during PEM-Tropics B are much lower than during PEM-Tropics A in the upper tertile of C_2H_2 but are similar in the lower tertile of C_2H_2. The overestimate of HNO_3 is unlikely caused by long-range transport for the lower and middle tertiles of C_2H_2 because the chemical lifetime of PAN is longer than HNO_3 in the upper troposphere.

Figure 11

Nitric acid and PAN are longer lived than NO_x. Their decomposition to NO_x is very slow in the upper troposphere. The loss of these reservoirs is not due to chemistry but downward transport associated with the subsidence branch of convection. The loss of HNO_3 and PAN in the upper troposphere cannot be compensated for by convective updrafts, in which HNO_3 is scavenged and PAN concentrations are very low. This loss of HNO_3 and PAN, and to a much smaller extent HNO_4 and N_2O_5, must be compensated for by chemical production from NO_x. Convective transport therefore dictates an upper tropospheric source of NO_x to make up for the loss. Figure 12 shows the simulated chemical production and loss rates of HNO_3 and PAN. Chemical production of HNO_3 exceeds loss throughout the troposphere reflecting wet scavenging of HNO_3. The net production of PAN above 5 km is compensated for by downward transport into the lower troposphere where PAN readily decomposes by thermolysis at warm temperatures and produces a large source of NO_x. In the model the source of NO_x from PAN decomposition in the lower troposphere is able to compensate for the loss due to wet and dry deposition of HNO_3 in the region. It is in the upper and middle troposphere (above 4 km) that a large source of NO_x of $4x10^8$ molecules

Figure 12

cm^{-2} s^{-1} is needed to account for the surplus in the chemical budgets of PAN and HNO_3. Extending this source over the tropics (20°S-20°N) yields a net source of 0.4 Tg N yr^{-1}. If we assume that N_2O_5 hydrolysis in aerosols or another NO_x to HNO_3 pathway is necessary to correct the underestimate of HNO_3 concentrations in the model, this tropical source of NO_x is at least 1 Tg N yr^{-1}.

Three possible venues could contribute to the needed NO_x sources, lightning over the oceans, transport of lightning NO_x from tropical continents, and long-rang transport of NO_x reservoirs (PAN and HNO_3). We have discussed previously that the third possibility may have contributed to PAN and HNO_3 concentrations in the upper tertile of C_2H_2 but not the lower tertiles. Given the inefficient decomposition rates in the upper troposphere (Figure 12), the source is unlikely to be significant. The lightning sources over the tropical ocean and land are difficult to distinguish on the basis of anthropogenic chemical tracers because fossil fuel and industrial emissions are weak in the tropics. Examination of high-NO_x encounters during PEM-Tropics B often leads to oceanic cumulus clouds in GEOS satellite images a few days back along the air trajectories calculated by *Fuelburg et al.* [this issue]. Even if only half of the source (0.2-0.5 Tg N yr^{-1}) is due to marine lightning, it is significantly large considering that the global lightning sources have been estimated to be as small as 3 Tg N yr^{-1} in 3-D models [e.g., *Levy et al.*, 1996; *Wang et al.*, 1998a]. The lightning parameterization in global 3-D models [e.g., *Price and Rind*, 1992] generally predicts lightning frequencies orders of magnitudes smaller over the ocean than over land. Future studies on the NO_x source from marine lightning are warranted.

4.4. Free Tropospheric DMS and SO_2

Dimethylsulfide in the atmosphere is oxidized mostly by OH and to a lesser extent by NO_3 [*Berresheim et al.*, 1995]. Whereas the rate constants for H abstraction reaction by the radicals are reasonably known, kinetics data for the adduct reaction of DMS and OH are uncertain [*DeMore et al.*, 1997]. While the former reaction is bimolecular, the latter reaction involves the DMS-OH adduct that either decomposes or reacts with O_2 and hence is more complex. The bulk rate constants for the adduct reaction were derived by *Hynes et al.* [1986] for near surface atmospheric conditions. Their empirical fitting function has since been widely adopted [e.g., *Atkinson et al.*, 1997]. *Hynes et al.* [1995] and *Barone et al.* [1996] undertook two more recent experiments that probed elementary reactions at low pressures and temperatures. For DMS oxidation in the free troposphere the recent works are more pertinent. We derive new rate constants for the adduct reaction on the basis of *Hynes et al.* [1995] and *Barone et al.* [1996]. The reaction sequence is

(R1) $OH + DMS \rightarrow DMS\text{-}OH$

(R2) $DMS\text{-}OH \rightarrow DMS + OH$

(R3) $DMS\text{-}OH + O_2 \rightarrow$ products

The equilibrium constant for reactions (R1) and (R2) is

$$K_c = k_1/k_2 \ . \qquad (1)$$

Hynes et al. [1995] and *Barone et al.* [1996] derived K_c values from their measurements at 250-267 and 228-234 K, and 30-100 and 100 Torr, respectively. Fitting these data, we obtain

$$K_c = 2.7\text{x}10^{-26} \exp(5133/T) \text{ cm}^3 \text{ molecule}^{-1}. \qquad (2)$$

There is a slight temperature dependence of k_1 [*Barone et al.*, 1996]. We apply a generic formulation $k_1 = A_1 * \exp(200/T)$ [*DeMore et al.*, 1997] to fit the experimental data and obtain

$$k_1 = 3.2\text{x}10^{-12} \exp(200/T) \text{ cm}^3 \text{ molecule}^{-1} \text{ s}^{-1} \qquad (3)$$

and hence

$$k_2 = 1.2\text{x}10^{14} \exp(-4933/T) \text{ s}^{-1} \ , \qquad (4)$$

where T is in Kelvin. *Barone et al.* [1996] also showed pressure dependence of k_1 and k_2. We include this uncertainty by assuming a linear pressure dependence to compute another set of rate constants k', i.e., $k'_1 = k_1 * (P/100)$ and $k'_2 = k'_2 * (P/100)$, where P is in Torr.

For the value of k_3, *Hynes et al.* [1995] and *Barone et al.* [1996] found it to be independent of T and P at $8\text{x}10^{-13}$ and $10\text{x}10^{-13}$ cm^3 molecule^{-1} s^{-1}, respectively. We adopt $k_3 = 9\text{x}10^{-13}$ cm^3 molecule^{-1} s^{-1}. We therefore derive a rate expression for the adduct channel,

$$k_{ad} = \frac{2.4 \times 10^{-38} \exp(5133/T)}{1 + 7.5 \times 10^{-27} \exp(4933/T)[O_2]} \qquad (5)$$

and with a linear pressure dependence of k'_1 and k'_2,

$$k'_{ad} = \frac{2.4 \times 10^{-38} \exp(5133/T)}{1 + 7.5 \times 10^{-25} \exp(4933/T)([O_2]/P)} \qquad (6)$$

where k_{ad} *and* k'_{ad} are in cm^3 molecule^{-1} s^{-1}, T is in Kelvin, and P is in Torr.

Figure 13

Figure 13 compares these rate constants to those for the abstraction channel and the addition reaction rate constants by *Hynes et al.* [1986]. The H-abstraction rate constant decreases with altitude while the addition rate constant generally increases; the latter channel is more important or even dominant in the free troposphere. The DMS-OH adduct reaction accounts for 20, 30, and 40% in boundary layer and 75, 60, and 75% at 8 km, respectively, for the rate constants by *Hynes et al.* [1986] and of (5) and (6). Equation (6) with the pressure dependence is expected to give faster rate constants than (5). The relatively good agreement between that from *Hynes et al.* [1986] and (6) in the free troposphere is fortuitous since the rate expression given by *Hynes et al.* [1986], strictly speaking, applies only for 1 atmosphere pressure whereas (6) is pressure dependent. The new measurements at low pressures and temperatures imply higher branching ratios for the addition channel in the boundary layer than predicted by *Hynes et al.* [1986]. Our primary interest is in DMS and SO_2 concentrations in the free troposphere. We will adopt in our 1-D simulations equations (5) and (6) to bracket the range of addition rate constants.

In the simulation of DMS we specify its concentration at

500 m as observed. The resulting DMS concentrations in the free troposphere reflect the source from convective transport compensated for by oxidation by OH and NO_3. Figure 14 shows that 50-90% of the observations are below the LOD at altitudes above 3 km, where the model predicts concentrations of 5-10 pptv. The observed medians in the free troposphere are lower than plotted values since we used the LOD value as an upper limit for data bins with LOD fraction > 50%. To narrow the possible causes for the large model overestimates, further measurements on the kinetics of DMS+OH adduct reaction are necessary. The chemical lifetime of DMS is less than 1 day in the upper troposphere. The concentrations of DMS are therefore more susceptible to sometimes highly elevated OH concentrations observed around convective systems [e.g., *Jaeglé et al.*, 1997]. It is also possible that DMS is oxidized in the free troposphere by processes other than reactions with OH and NO_3.

Figure 14

The virtually unobservable level of DMS in the free troposphere, at first sight, implies that DMS cannot be a major source of SO_2 outside the boundary layer. This issue is further masked by other sources apparently making contributions to free tropospheric SO_2 including anthropogenic and volcanic sources [*Thornton et al.*, 1999]. However, convection can transport into the free troposphere large amounts of insoluble DMS. It is reasonable to assume that SO_2 is produced from transported DMS in the free troposphere. The yields of SO_2 from DMS oxidation are yet another uncertainty [e.g., *Davis et al.*, 1999]. We adopt oxidation yields of 1 for OH and NO_3 abstraction reactions and 0.6 for the DMS-OH adduct reaction [*Davis et al.*, 1999; *Koch et al.*, 1999]. Figure 15 shows the observed median SO_2 profile and model results using the rate expressions of (5) and (6), respectively. To simplify the interpretation of the model results, we assume a complete scavenging of SO_2 during convective transport and specify the SO_2 concentration at 500 m as observed. The latter led to the kink at 500 m in the model results. These measures ensure that free tropospheric SO_2 simulated in the model are produced from DMS oxidation. The difference in the yield of SO_2 between the abstraction and addition channels is reflected in the general decrease of model simulated SO_2 concentrations with altitude as the addition channel becomes more important (Figure 13). It is also reflected in the lower SO_2 concentrations obtained using the faster rate expression of (6) than using that of (5) for the addition channel. Model results suggest that convective transport of DMS from the boundary layer could explain the observed level of SO_2 concentrations in the free troposphere over the tropical Pacific.

Figure 15

5. Conclusions

We analyzed observations from PEM-Tropics B to investigate factors controlling O_3-HO_x-NO_x and SO_2 chemistry over the tropical Pacific. Interesting comparisons can be made with PEM-Tropics A observations, which were strongly influenced by biomass burning outflow. During PEM-Tropics B, C_2H_2 correlated well with C_2Cl_4, an industrial tracer, reflecting long-range transport of pollutants from northern industrial continents. No such correlation was found for biomass-burning dominated PEM-Tropics A. The degree of influence, for

which we examined data groups categorized by tertiles of C_2H_2, varied drastically between the two missions. Whereas CO concentrations were enhanced significantly from the lower to upper tertile of C_2H_2 in both missions, enhancements in O_3 and NO_x concentrations were hard to find during PEM-Tropics B in contrast to the large increases observed during PEM-Tropics A. Concentrations of NO_x, in fact, showed a decrease from the upper to lower tertiles of C_2H_2 during PEM-Tropics B. The differences reflect longer timescales of transport during PEM-Tropics B than A, resulting in the depletion of shorter-lived O_3 and NO_x. The large enhancements in longer-lived CO and hydrocarbons but not in O_3 and NO_x depressed OH concentrations in air masses influenced by industrial outflow over the tropical Pacific. In contrast, OH concentrations over the tropical Pacific were enhanced in air masses influenced by biomass burning outflow during PEM-Tropics A because the shorter timescale of transport allowed for enhanced O_3 and NO_x concentrations. Transport of pollutants from different source regions during PEM Tropics A and B therefore showed opposite effects on the oxidizing capacity of the atmosphere (defined largely by OH concentrations) over the tropical Pacific. The observed tendency of pollutant outflow to enhance OH concentrations near the source regions and reduce OH concentrations afar is consistent with the global 3-D model result by Wang and Jacob [1988] that fossil fuel and industrial emissions in general boost OH concentrations in the northern hemisphere while depressing OH in the southern hemisphere.

Convection during PEM-Tropics B was more vigorous than during PEM-Tropics A. Using CH_3I as a tracer for convective transport in a 1-D model, we found a turnover timescale of 10 days by convection during PEM-Tropics B, twice as fast as during PEM-Tropics A. Observations of CH_3I from PEM-Tropics A and B suggest that convective outflow in the tropics is evenly distributed with altitude up to the DC-8 flight ceiling of 12 km, implying stronger outflow in the middle troposphere than predicted in a general circulation model [*Wang et al.*, 2000]. Observations of CH_3I above 12 km are necessary to examine if such a distribution profile of convective outflow extends into the top layer of the tropical troposphere.

Model simulated HO_2, CH_2O, H_2O_2, CH_3OOH, and PAN concentrations showed reasonable agreement with the observations. Although simulated CH_2O concentrations are consistently higher by ~25 pptv than observed medians, this level of agreement is still noteworthy in light of large discrepancies found in previous field campaigns. Proper care needs to be taken to account for CH_2O data below the LOD. Despite of the good agreement for HO_2, model simulated OH concentrations were consistently lower (~25%) than observations above 6 km. The agreement between simulated and observed peroxides is not as good as that for PEM-Tropics A; model simulated CH_3OOH are consistently higher by ~100 pptv. The discrepancies between simulated and observed OH and peroxides are, however, within the measurement uncertainties. Unlike the model overestimates of HNO_3 in previous studies, simulated HNO_3 concentrations during PEM-Tropics B were much lower than observations. Invoking N_2O_5 hydrolysis in aerosols could mitigate the underestimates. It is, however, difficult to reconcile the difference between PEM-Tropics A and B. Dur-

ing PEM-Tropics A the model predicted concentrations of HNO_3 close to or moderately higher than the observations without invoking N_2O_5 hydrolysis in aerosols.

The comparatively faster convective transport and less influence from long-range transport of pollutants during PEM-Tropics B than A makes PEM-Tropics B a good case for studying the effects of convection on chemistry over the tropics. Convective transport of CH_3OOH was the dominant primary HO_x source above 10 km. The corresponding increase in HO_x and O_3 production in the upper troposphere was offset by the decrease in the lower and middle troposphere due to convective scavenging of another HO_x reservoir, H_2O_2. Convective transport increased column O_3 production by 4% but decreased column HO_x production and OH concentrations by 7 and 4%, respectively. We could not analyze the effect of convection on enhancing H_2O concentrations in our model. Convection could in this sense be a primary driver for HO_x chemistry in the tropical troposphere since the reaction of $O(^1D)$ and H_2O provides the dominant primary HO_x source in the middle and lower troposphere.

The column budget of O_3 had a large deficit; column production was only half of the loss. The deficit is likely compensated for by transport of O_3 from other regions of the tropics since transport from northern industrial continents had little impact on O_3 and NO_x concentrations. Convective transport of reactive nitrogen also imposed a budget deficit of NO_x. The loss of upper tropospheric HNO_3 and PAN due to the subsiding branch of convection could not be compensated for by the ascending branch because of convective scavenging of HNO_3 and very low concentrations of PAN in the lower troposphere. In the lower troposphere, thermal decomposition of PAN transported by subsidence provided the necessary NO_x source to account for scavenging and deposition of HNO_3. The implied NO_x source in the free troposphere (above 4 km) is 0.4-1 Tg N yr^{-1} over the tropics (20°S - 20°N). The likely sources are in situ marine lightning or transport of NO_x from continental lightning. The former source is supported by GEOS observations of marine cumulus clouds along the calculated back trajectories of high NO_x encounters. The magnitude of this source highlights the need to understand NO_x production by marine lightning.

Concentrations of DMS were barely detectable in the free troposphere with 60%-100% observational data below the LOD (1 pptv). The widely adopted rate constants by *Hynes et al.* [1986] were measured for atmospheric conditions near the surface. For free tropospheric studies, we derived new rate constants for the DMS-OH adduct reaction on the basis of recent kinetics data at low pressures and temperatures by *Hynes et al.* [1995] and *Barone et al.* [1996]. A large uncertainty in the new rate constants is the pressure dependence of k_1. We adopted one pressure-independent rate expression and one with a linear pressure dependence between 100 and 760 Torr as the lower and upper limits, respectively. Convective transport supplied far higher DMS concentrations in the free troposphere in the model than were observed. Either abnormal enhancements of OH concentrations around convective events observed in previous field campaigns or oxidation mechanisms other than reaction with OH and NO_3 are necessary to explain the observed low DMS concentrations in the tropical

free troposphere. Our results suggest that caution must be exercised when using observed very low concentrations of DMS as evidence of little contribution by DMS to free tropospheric SO_2. Although more work is needed to clarify potential DMS oxidation pathways, it is clear that the amount of DMS transported by convection was large enough to explain observed SO_2 concentrations in the free troposphere over the tropical Pacific.

Acknowledgments. We thank Anthony Hynes for helpful comments on sulfur chemistry and William Grant and Gao Chen for their suggestions. We thank Francois Ravetta and Daniel Jacob for providing the merged data files used in this work and anonymous reviewers for their comments. This work was supported in part by the National Aeronautics and Space Administration Global Tropospheric Experiment Program. The contribution of PHW was supported by the National Science Foundation through grant ATM-9910912.

References

Atkinson, R., et al., Evaluated kinetic and photochemical data for atmospheric chemistry, *J. Phys. Chem. Ref. Data*, *26*, suppl. VI, 1329-1499, 1997.

Barone, S. B., A. A. Turnipseed, and A. R. Ravishankara, Reaction of OH with dimethyl sulfide (DMS), 1, Equilibrium constant for OH+DMS reaction and the kinetics of the OH·DMS+O_2 reaction, *J. Phys. Chem.*, *100*, 14,694-14,702, 1996.

Berresheim, H., P. Wine, and D. D. Davis, Sulfur in the Atmosphere, in *Composition, Chemistry, and Climate of the Atmosphere*, edited by H. B. Singh, pp. 251-307, Van Nostrand Reinhold, New York, 1995.

Blake, N. J., et al., Influence of southern hemispheric biomass burning on mid-tropospheric distributions of nonmethane hydrocarbons and selected halocarbons over the remote South Pacific, *J. Geophys. Res.*, *104*, 16,213-16,232, 1999.

Blake, N. J., et al., Large-scale latitudinal and vertical distributions of NMHCs and selected halocarbons in the troposphere over the tropical Pacific Ocean during the March-April 1999 Pacific Exploratory Mission (PEM-Tropics B), *J. Geophys. Res.*, this issue.

Browell, et al., Large-scale air mass characteristics observed over the remote tropical Pacific Ocean during March-April 1999: Results from PEM Tropics-B field experiment, *J. Geophys. Res.*, this issue.

Charlson, R. J., J. E. Lovelock, M. O. Andreae, and S. G. Warren, Oceanic phytoplankton, atmospheric sulfur, cloud albedo, and climate, *Nature*, *326*, 655-661, 1987.

Chatfield, R. B., Anomalous HNO_3/NO_x ratio of remote tropospheric air: Conversion of nitric acid to formic acid and NO_x?, *Geophys. Res. Lett.*, *21*, 2705-2708, 1994.

Cohan, D. S., M. G. Schultz, D. J. Jacob, B. G. Heikes, and D. R. Blake, Convective injection and photochemical decay of peroxides in the upper troposphere: Methyl iodide as a tracer of marine convection, *J. Geophys. Res.*, *104*, 5717-5724, 1999.

Crawford, J. H., et al., Implications of large scale shifts in tropospheric NO_x levels in the remote tropical Pacific, *J. Geophys. Res.*, *102*, 28,447-28,468, 1997.

Davis, D. D., J. Crawford, S. Liu, S. McKeen, A. Bandy, D. Thornton, and D. Blake, Potential impact of iodine on tropospheric levels of ozone and other critical oxidants, *J. Geophys. Res.*, *101*, 2135-2147, 1996.

Davis, D., et al., Dimethyl sulfide oxidation in the equatorial Pacific: Comparison of model simulations with field observations for DMS, SO_2, H_2SO_4 (g), MSA(g), MS, NSS, *J. Geophys. Res.*, *104*, 5665-5784, 1999.

Davis, D. D., et al., Marine latitude/altitude OH distributions: Comparison of Pacific Ocean observations with models, *J. Geophys. Res.*, this issue.

DeMore, W. B., et al., Chemical kinetics and photochemical data for use in stratospheric modeling, *JPL Publ. 97-4*, 266 pp., 1997.

Faloona, I., et al., Observations of HO_x and its relationship with NO_x in the upper troposphere during SONEX, *J. Geophys. Res.*, *105*, 3771-3783, 2000.

Fan, S.-M., D. J. Jacob, D. L. Mauzerall, J. D. Bradshaw, S. T. Sandholm, D. R. Blake, H. B. Singh, R. W. Talbot, G. L. Gregory, and G. W. Sachse, Origin of tropospheric NO_x over subarctic eastern Canada in summer, *J. Geophys. Res.*, *99*, 16,867-16,877, 1994.

Fried, A., et al., Photochemistry of formaldehyde during the 1993 Tropospheric OH Photochemistry Experiment, *J. Geophys. Res.*, *102*, 6283-6296, 1997.

Fuelberg, H. E., et al., A meteorological overview of the PEM-Tropics B period, *J. Geophys. Res.*, this issue.

Hauglustaine, D. A., G. P. Brasseur, S. Walters, P. J. Rasch, J. F. Müller, L. K. Emmons, and M. A. Carroll, MOZART, a global chemical transport model for ozone and related chemical tracers, 2, Model results and evaluation, *J. Geophys. Res.*, *103*, 28,291-28,335, 1998.

Hoell, J. M., D. D. Davis, D. J. Jacob, M. O. Rodgers, R. E. Newell, H. E. Fuelberg, R. J. McNeal, J. L. Raper, and R. J. Bendura, The Pacific Exploratory Mission in the tropical Pacific: PEM-Tropics A, August-September 1996, *J. Geophys. Res.*, *104*, 5567-5583,

1999.
Holton, J. R., P. H. Haynes, M. E. McIntyre, A. R. Douglass, R. B. Rood, and L. Pfister, Stratosphere-troposphere exchange, *Rev. Geophys., 33*, 403-439, 1995.
Hynes, A. J., P. H. Wine, and D. H. Semmes, Kinetics and mechanism of OH reactions with organic sulfides, *J. Phys. Chem., 90*, 4148-4156, 1986.
Hynes, A. J., R. B. Stoker, A. J. Pounds, T. McKay, J. D. Bradshaw, J. M. Nicovich, and P. H. Wine, A mechanistic study of the reaction of OH with Dimethyl-d_6 sulfide: Direct observation of adduct formation and the kinectics of the adduct reaction with O_2, *J. Phys. Chem., 99*, 16,967-16,975, 1995.
Intergovernmental Panel on Climate Change (IPCC), *Climate Change 1995, The Science of Climate Change*, edited by J. T. Houghton et al., 572 pp., Cambridge Univ. Press, New York, 1996.
Jaeglé, L., et al., Observed OH and HO_2 in the upper troposphere suggest a major source from convective injection of peroxides, *Geophys. Res. Lett., 24*, 3181-3184, 1997.
Jacob, D. J., et al., Origin of ozone and NO_x in the tropical troposphere: A photochemical analysis of aircraft observations over the South Atlantic basin, *J. Geophys. Res., 101*, 24,235-24,250, 1996.
Koch, D., D. J. Jacob, I. Tegen, D. Rind, and M. Chin, Tropospheric sulfur simulation and sulfur direct radiative forcing in the Goddard Institute for Space Studies general circulation model, *J. Geophys. Res., 104*, 23,799-23,822, 1999.
Lawrence, M. G., and P. J. Crutzen, The impact of cloud particle gravitational settling on soluble trace gas distributions, *Tellus, Ser. B, 50*, 263-289, 1998.
Levy H., II., W.J. Moxim, and P.S. Kasibhatla, A global 3-dimensional time-dependent lightning source of NO_x, *J. Geophys. Res., 101*, 22911-22922, 1996.
Liu, S. C., J. R. McAfee, and R. J. Cicerone, Radon 222 and tropospheric vertical transport, *J. Geophys. Res., 89*, 7291-7297, 1984.
McCulloch, A., and P. M. Midgley, The production and global distribution of emissions of trichloroethene, tetrachloroethene and dichloromethane over the period of 1988-1992, *Atmos. Environ., 30*, 601-608, 1996.
McKeen, S. A., et al., Photochemical modeling of hydroxyl and its relationship to other species during the Tropospheric OH Photochemistry Experiment, *J. Geophys. Res., 102*, 6467-6493, 1997.
Müller, J.-F., and G. Brasseur, Sources of upper tropospheric HO_x: A three-dimensional study, *J. Geophys. Res., 104*, 1705-1715, 1999.
Olson, J. A., et al., Seasonal differences in the photochemistry of the South Pacific: A comparison of observations and model results from PEM-Tropics A and B, *J. Geophys. Res.*, this issue.
Prather, M. J., and D. J. Jacob, A persistent imbalance in HO_x and NO_x photochemistry of the upper troposphere driven by deep tropical convection, *Geophys. Res. Lett., 24*, 3189-3192, 1997.
Price, C. and D. Rind, A simple lightning parameterization for calculating global lightning distributions, *J. Geophys. Rev., 97*, 9919-9933, 1992.
Raper, J. L., M. M. Kleb, D. J. Jacob, D. D. Davis, R. E. Newell, H. E. Fuelberg, R. J. Bendura, J. M. Hoell, and R. J. McNeal, Pacific Exploratory Mission in the tropical Pacific: PEM-Tropics B, March-April 1999, *J. Geophys. Res.*, this issue.
Sander, S. P., et al., Chemical kinetics and photochemical data for use in stratospheric modeling - Supplement to Evaluation 12: Update of key reactions, *JPL Publ. 00-3*, 74 pp., 2000.
Schultz, M., et al., On the origin of tropospheric ozone and NO_x over the tropical South Pacific, *J. Geophys. Res., 104*, 5829-5843, 1999.
Schultz, M., D. J. Jacob, J. D. Bradshaw, S. T. Sandholm, J. E. Dibb, R. W. Talbot, and H. B. Singh, Chemical NO_x budget in the upper troposphere over the tropical South Pacific, *J. Geophys. Res., 105*, 6669-6679, 2000.
Singh, H. B., D. O'Hara, D. Herlth, W. Sachse, D. R. Blake, J. D. Bradshaw, M. Kanakidou, and P. J. Crutzen, Acetone in the atmosphere: Distribution, sources, and sinks, *J. Geophys. Res., 99*, 1805-1819, 1994.
Singh, H. B., Y. Chen, A. C. Staudt, D. J. Jacob, D. R. Blake, B. G. Heikes, and J. Snow, Evidence from the South Pacific troposphere for large global abundances and sources of oxygenated organic compounds, *Nature, 410*, 1078-1081, 2001.

Talbot, R. W., J. E. Dibb, E. M. Scheuer, D. R. Blake, N. J. Blake, G. L. Gregory, G. W. Sachse, J. B. Bradshaw, S. T. Sandholm, and H. B. Singh, Influence of biomass combustion emissions on the distribution of acidic trace gases over the southern Pacific basin during austral springtime, *J. Geophys. Res.*, *104*, 5623-5634, 1999.

Tan, D., et al., OH and HO2 in the Remote Tropical Pacific: Results from PEM-Tropics B, *J. Geophys. Res.*, this issue.

Thornton, D. C., A. R. Bandy, B. W. Blomquist, A. R. Driedger, and T. P. Wade, Sulfur dioxide distribution over the Pacific Ocean 1991-1996, *J. Geophys. Res.*, *104*, 5845-5854, 1999.

Trainer, M., E. Y. Hsie, S. A. McKeen, T. Tallamraju, D. D. Parish, F. C. Fehsenfeld, and S. C. Liu, Impact of natural hydrocarbons on hydroxyl and peroxy radicals at a remote site, *J. Geophys. Res.*, *92*, 11,879-11,894, 1987.

Trainer, M., et al., Observations and modeling of the reactive nitrogen photochemistry at a rural site, *J. Geophys. Res.*, *96*, 3045-3063, 1991.

Wang, Y., and D. J. Jacob, Anthropogenic forcing on tropospheric O_3 and OH since preindustrial times, *J. Geophys. Res.*, *103*, 31,123-31,136, 1998.

Wang, Y., D. J. Jacob, and J. A. Logan, Global simulation of tropospheric O_3-NO_x-hydrocarbon chemistry, 1, Model formulation, *J. Geophys. Res.*, *103*, 10,713-10,725, 1998a.

Wang, Y., J. A. Logan, and D. J. Jacob, Global simulation of tropospheric O_3-NO_x-hydrocarbon chemistry, 2, Model evaluation and global ozone budget, *J. Geophys. Res.*, *103*, 10,727-10,755, 1998b.

Wang, Y., D. J. Jacob, and J. A. Logan, Global simulation of tropospheric O_3-NO_x-hydrocarbon chemistry, 3. Origin of tropospheric ozone and effects of non-methane hydrocarbons, *J. Geophys. Res.*, *103*, 10,757-10,768, 1998c.

Wang Y., S. C. Liu, H. Yu, S. Sandholm, T.-Y. Chen, and D. R. Blake, Influence of convection and biomass burning on tropospheric chemistry over the tropical Pacific, *J. Geophys. Res.*, *105*, 9321-9333, 2000.

[1]Department of Environmental Sciences, Rutgers University, New Brunswick, New Jersey.
[2]School of Earth and Atmospheric Sciences, Georgia Institute of Technology, Atlanta, Georgia.
[3]Now at Academia Sinica, Taipei, Taiwan.
[4]Also at School of Chemistry and Biochemistry, Georgia Institute of Technology, Atlanta, Georgia.
[5]National Center for Atmospheric Research, Boulder, Colorado.
[6]NASA Langley Research Center, Hampton, Virginia.
[7]Department of Chemistry, University of California at Irvine, Irvine, California.
[8]Department of Meteorology, Pennsylvania State University, University Park, Pennsylvania.
[9]Graduate School of Oceanography, University of Rhode Island, Narragansett, Rhode Island.
[10]NASA Ames Research Center, Moffett Field, California.
[11]Institute for the Study of Earth, Oceans, and Space, University of New Hampshire, Durham, New Hampshire.
[12]Now at School of Earth and Atmospheric Sciences, Georgia Institute of Technology, Atlanta, Georgia.

Paper number 2001JD900084.
0148-0227/01/2001JD900084$09.00

E. L. Atlas and R. E. Shetter, NCAR, PO Box 3000, Boulder, CO 80307.
M. A. Avery and G. W. Sachse, NASA Langley Research Center, Hampton, VA 23681.
D. R. Blake and N. J. Blake, Department of Chemistry, University of California, Irvine, CA 92697.
W. H. Brune, Department of Meteorology, Pennsylvania State University, University Park, PA 16802.
D. D. Davis, S. T. Sandholm, D. Tan, and P. W. Wine, School of Earth and Atmospheric Sciences, Georgia Institute of Technology, Altanta, GA 30332.
B. G. Heikes, Graduate School of Oceanography, University of Rhode Island, Narragansett, RI 02882.
S. C. Liu, Institute of Earth Sciences, Academia Sinica, Taipei, ROC 11529, Taiwan.
H. B. Singh, NASA Ames Research Center, Moffett Field, CA 94035.
R. W. Talbot, Institute for the Study of Earth, Oceans, and Space, University of New Hampshire, Durham, NH 03824.
Y. Wang, Department of Environmental Sciences, Rutgers University, 14 College Farm Road, New Brunswick, NJ 08901. (e-mail: yhw@envsci.rutgers.edu)

(Received September 7, 2000; revised January 21, 2001; accepted January 24, 2001.)

Table 1. Column O_3, OH, NO_x, NO_t, and Production of O_3[a]

Tertile of C_2H_2	O_3[b]	$P(O_3)$[c]	NO_x[d]	NO_t[e]	Observed OH[f]	Model OH[g]	24-hour OH[h]
Lower	10 (14)	1.3 (1.4)	2.1 (2.0)	10	2.87	2.55	1.27 (1.4)
Middle	11 (20)	1.2 (1.7)	2.0 (3.1)	12	2.59	2.25	1.12 (1.5)
Upper	12 (34)	1.1 (3.1)	1.6 (5.4)	14	2.30	1.94	0.96 (1.6)

[a] Integrated over the air column of 0-12 km (15°S-15°N). Observations are for solar zenith angle <85° excluding the return flights from Easter Island to California. Numbers in parenthesis are the corresponding values for PEM-Tropics A [*Wang et al.*, 2000]. The model is constrained by observed median concentrations of O_3, NO, CO, and hydrocarbons for the perspective tertiles of C_2H_2 (section 2).

[b] Observed medians in Dobson Unit (DU).

[c] Model computed 24-hour averages in 10^{11} molecules cm^{-3} s^{-1}.

[d] Model computed daytime averages constrained by observed NO concentrations in 10^{14} molecules cm^{-3}.

[e] Reactive nitrogen $NO_t = NO_x + PAN + HNO_3 + 2xN_2O_5 + HNO_4$, in 10^{14} molecules cm^{-3}. Column PAN and HNO_3 are measured medians. Daytime N_2O_5 and HNO_4 concentrations, ~5% of column NO_t, are from the model.

[f] Observed medians. Concentrations of OH are in 10^6 molecules cm^{-3}.

[g] Computed daytime averages.

[h] Computed 24-hour averages.

Figure Captions (Single Column)

Figure 1. Distribution of C_2Cl_4 concentrations as a function of C_2H_2 concentrations over the tropical Pacific (15°S-15°N) during PEM-Tropics A and B.

Figure 2. Observed median profiles of C_2H_2, CO, acetone, O_3, OH, and NO concentrations for the three tertiles of C_2H_2. The observations are binned vertically in 1-km intervals.

Figure 3. Observed and simulated daytime concentrations of CH_3I as a function of altitude. The solid line represents median concentrations in 1-km intervals; asterisks and horizontal bars represent means and standard deviations, respectively. Three model simulations are shown (see text for details). The concentration of CH_3I at 500 m is specified in the model as the observed median value at 0-1 km.

Figure 4. Observed and simulated daytime concentrations of OH, HO_2, and CH_2O as a function of altitude. Symbols for the observations are the same as in Figure 3. Observed medians, means, and standard deviations are shown for data bins with a LOD fraction <30% (the LOD limit (50 pptv) is assumed for LOD data); only median points (open triangles) are shown for data bins with a larger LOD fraction. When the LOD fraction is >50%, the LOD limit is used as the median. Model results are shown with and without convection.

Figure 5. The percentage fraction of observed CH_2O data points below the LOD as a function of altitude.

Figure 6. Same as Figure 4 but for H_2O_2 and CH_3OOH concentrations.

Figure 7. Simulated (24-hour average) primary HO_x sources as a function of altitude from $O(^1D)+H_2O$, photolysis of acetone, and photolysis of CH_3OOH and CH_2O transported from the lower troposphere by convection. The HO_x yield of CH_2O photolysis is computed on line.

Figure 8. Simulated (24-hour average) production rates of HO_x and O_3 as a function of altitude with and without convection.

Figure 9. Simulated (24-hour average) chemical production and loss rates of O_3 as a function of altitude.

Figure 10. Observed and simulated daytime concentrations of HNO_3 as a function of altitude for the three tertiles of C_2H_2. Symbols for the observations are the same as in Figure 3. The dotted line shows the results from the standard model. Median concentrations from P-3B measurements are shown by the long dashed line.

Figure 11. Same as Figure 10 but for PAN.

Figure 12. Same as Figure 9 but for HNO_3 and PAN.

Figure 13. Rate constants for the abstract and addition chan-

nels of the DMS+OH reaction as a function of altitude. Three rate constants are calculated for the addition channel (see text for details).

Figure 14. Observed and simulated daytime concentrations of DMS and the percentage fraction of observed DMS data points below the LOD (1 pptv) as a function of altitude. Symbols for the observations are the same as in Figure 3. As in Figure 4 for CH_2O, only median points (open triangles) are shown for data bins with >30% of data points below the LOD; when the LOD fraction is >50%, the LOD limit is used as the median. Two model results are shown using (5) and (6), respectively, for the rate constants of the DMS-OH adduct reaction. The concentration of DMS at 500 m is specified in the model as the observed median value at 0-1 km.

Figure 15. Same as Figure 14 but for SO_2. The concentration of SO_2 at 500 m is specified in the model as the observed median value at 0-1 km.

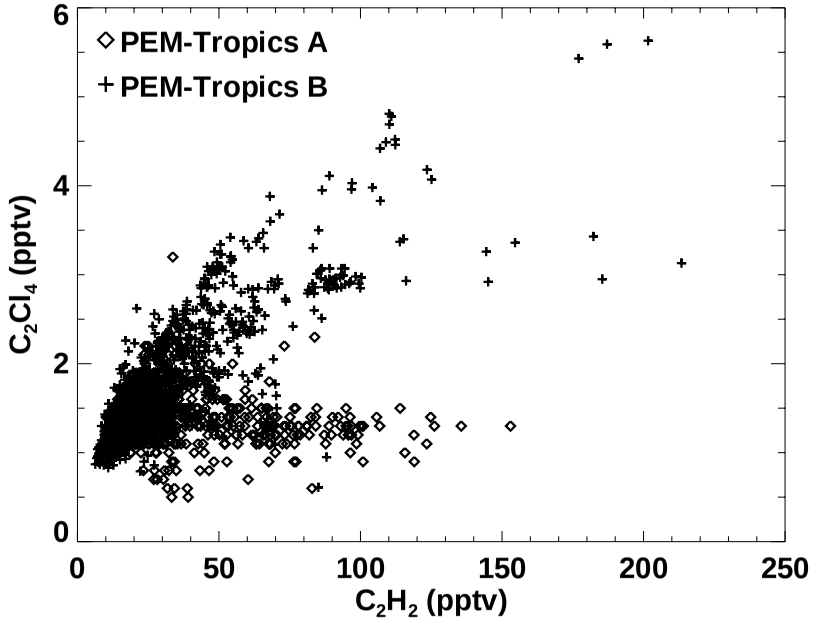

Figure 1 (Bottom)

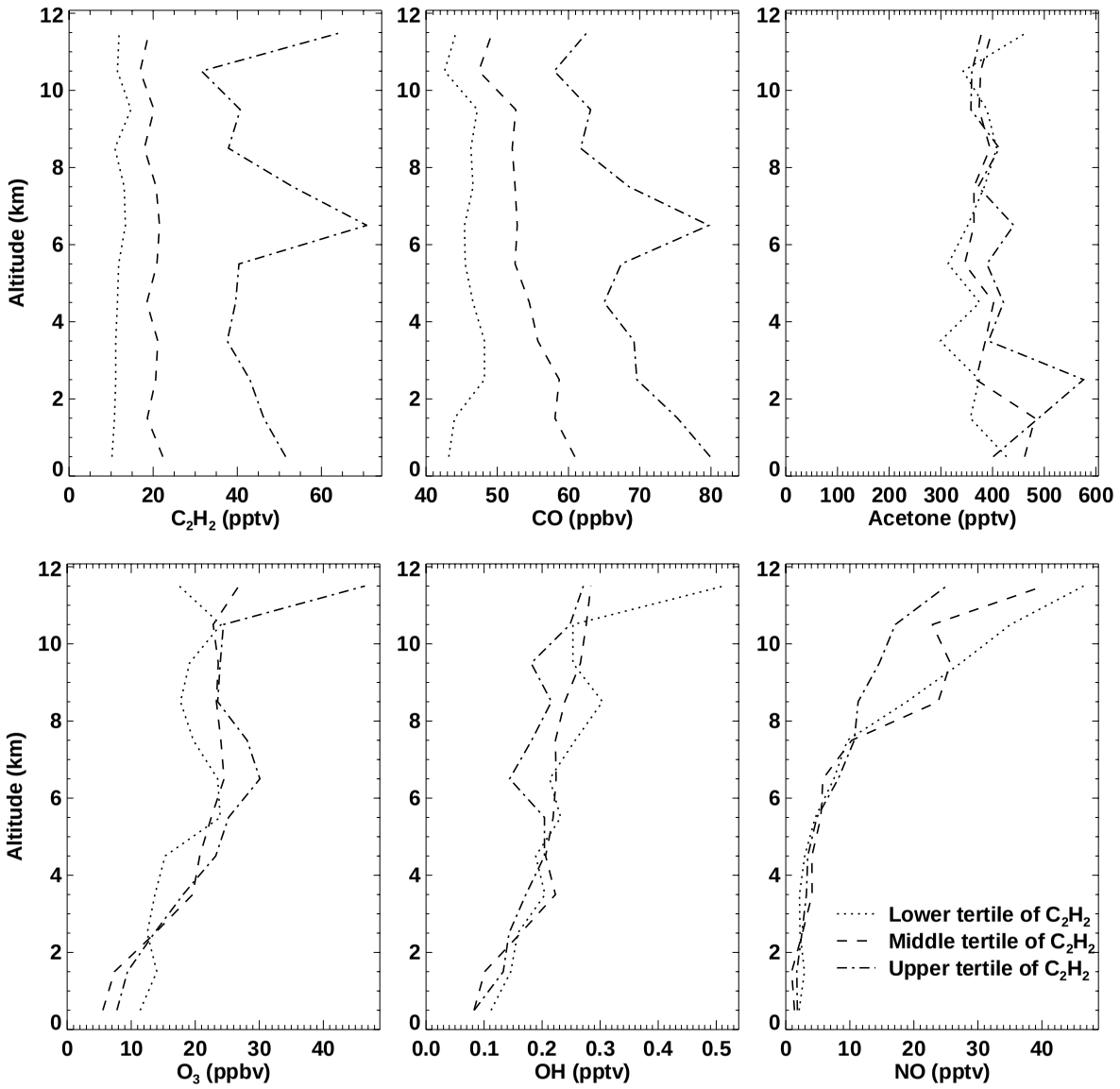

Figure 2 (Bottom)

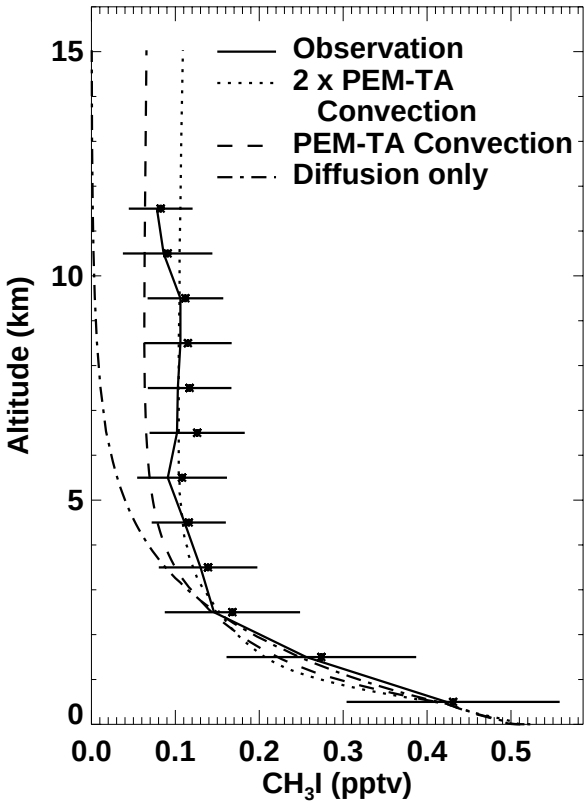

Figure 3 (Bottom)

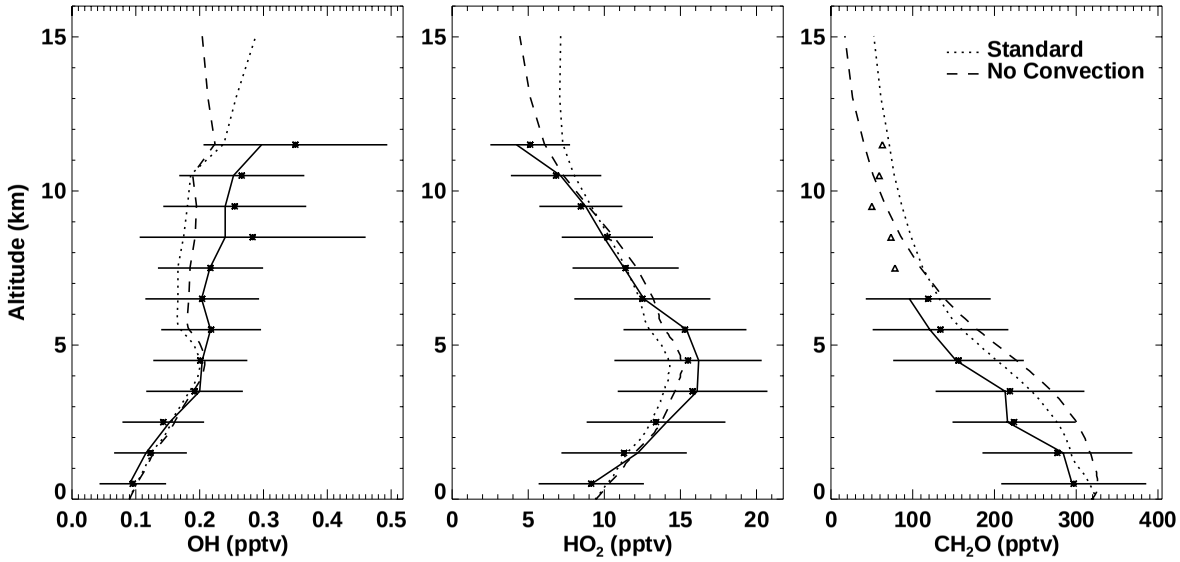

Figure 4 (Bottom)

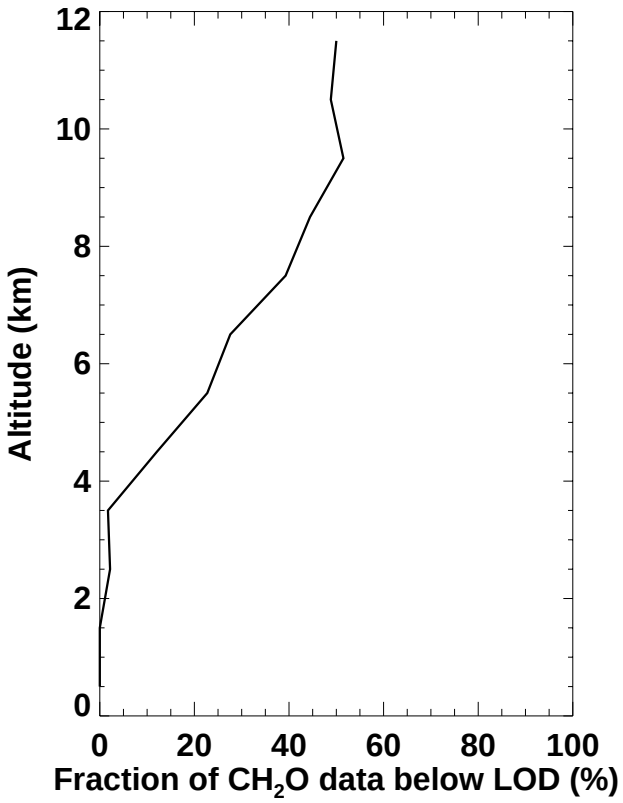

Figure 5 (Bottom)

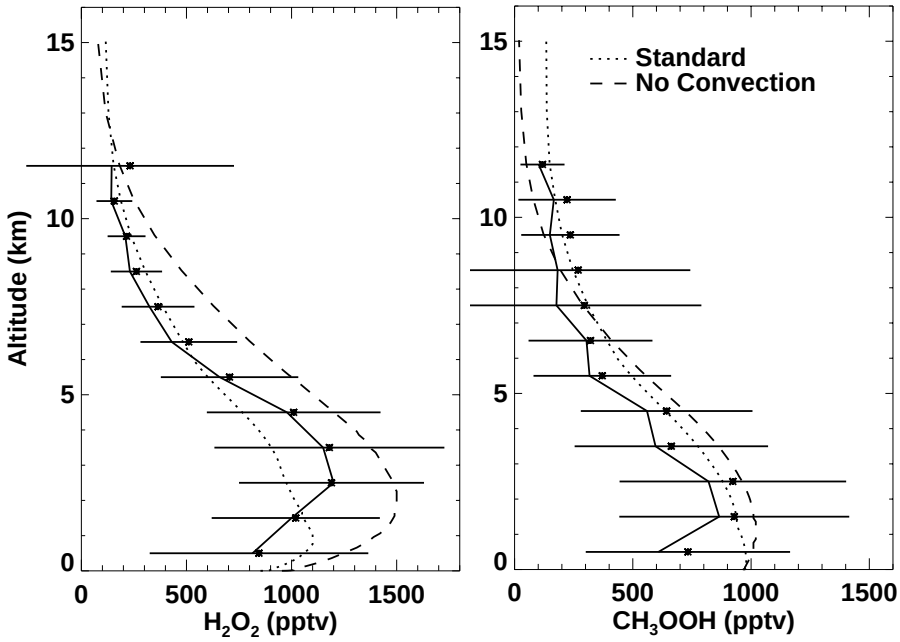

Figure 6 (Bottom)

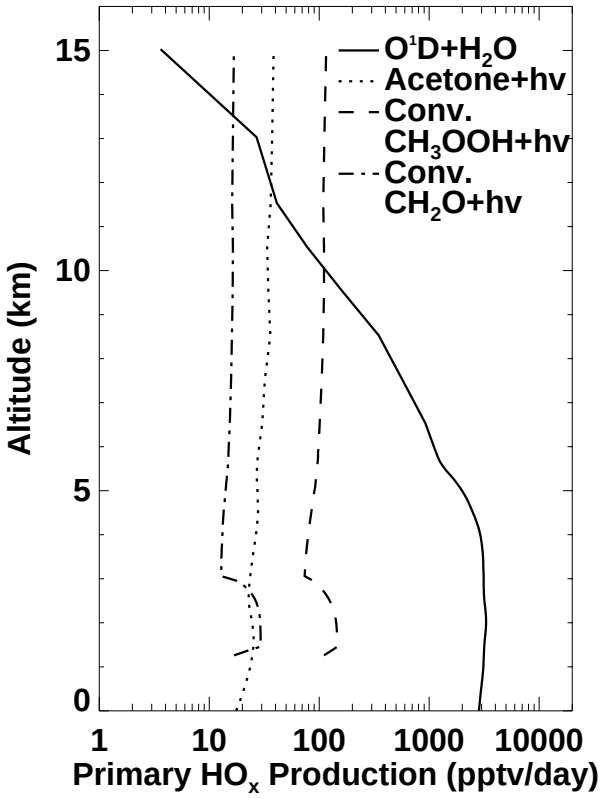

Figure 7 (Bottom)

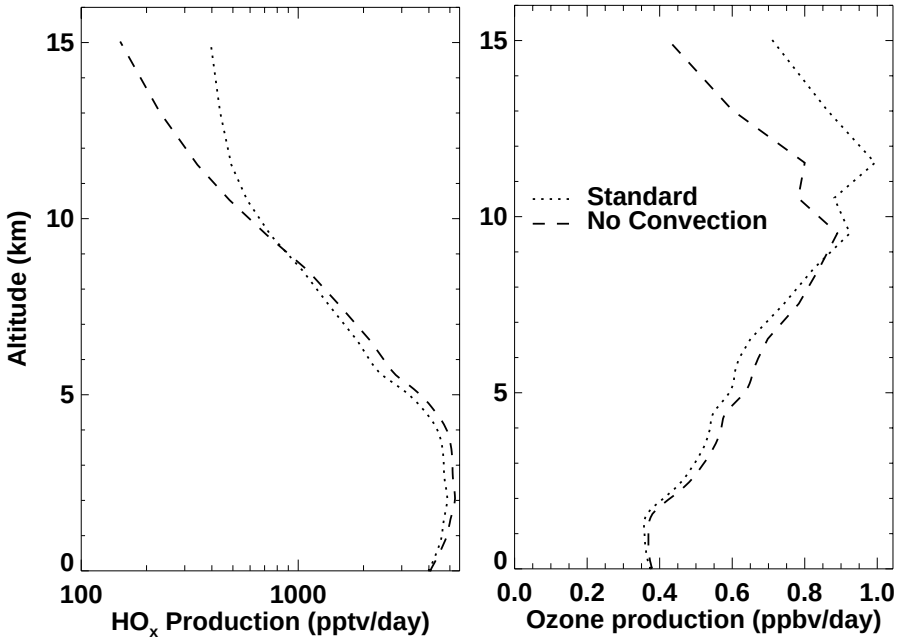

Figure 8 (Bottom)

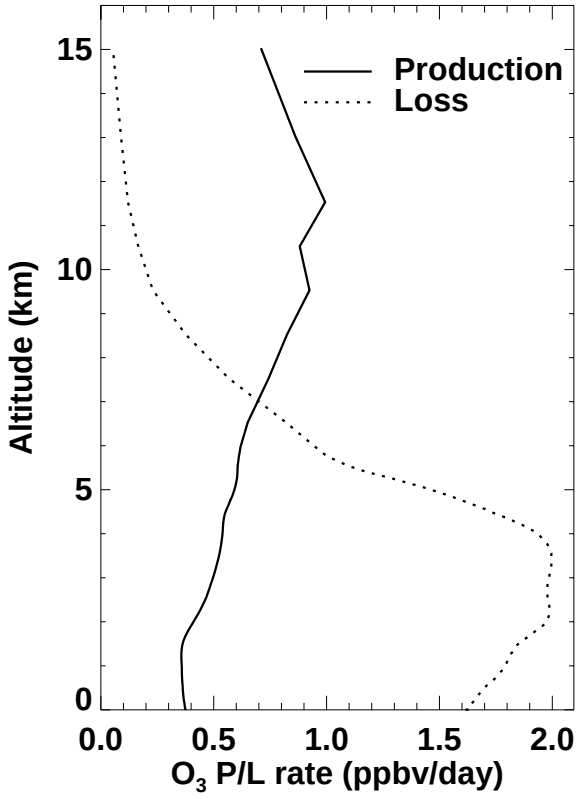

Figure 9 (Bottom)

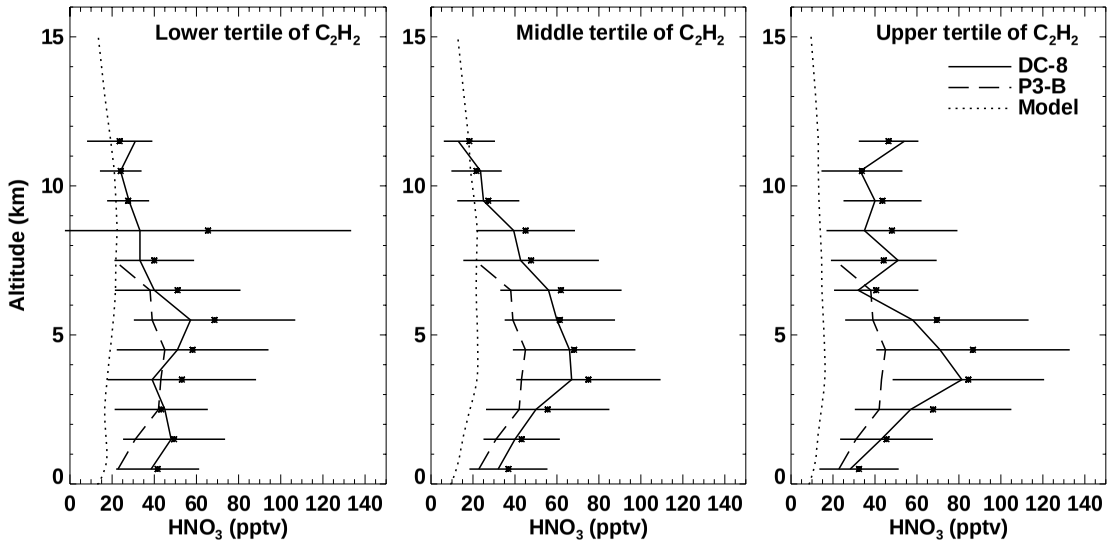

Figure 10 (Bottom)

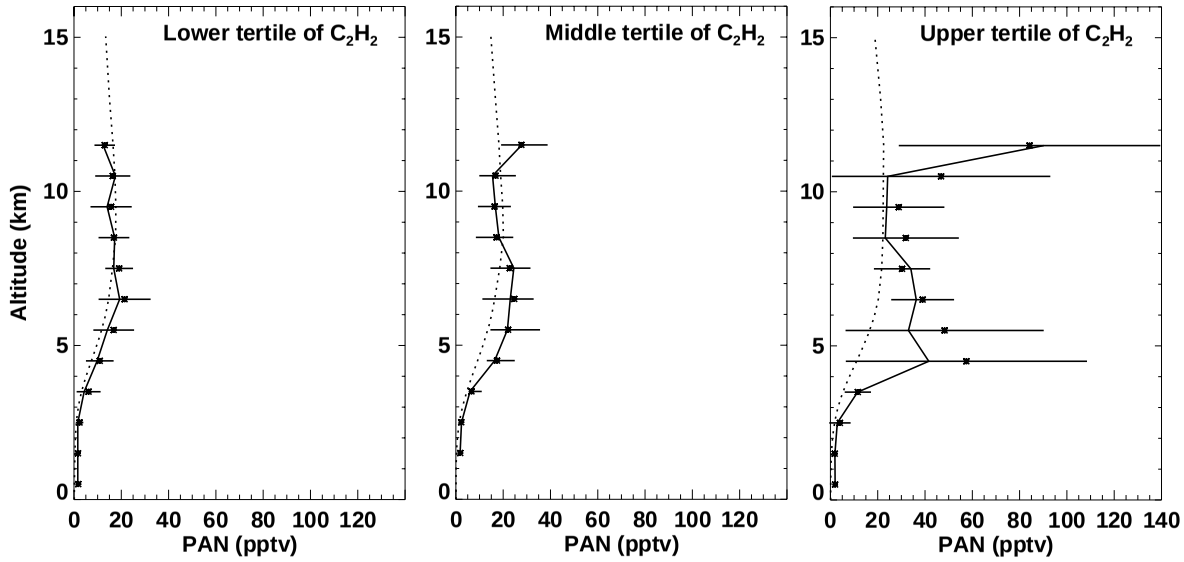

Figure 11 (Bottom)

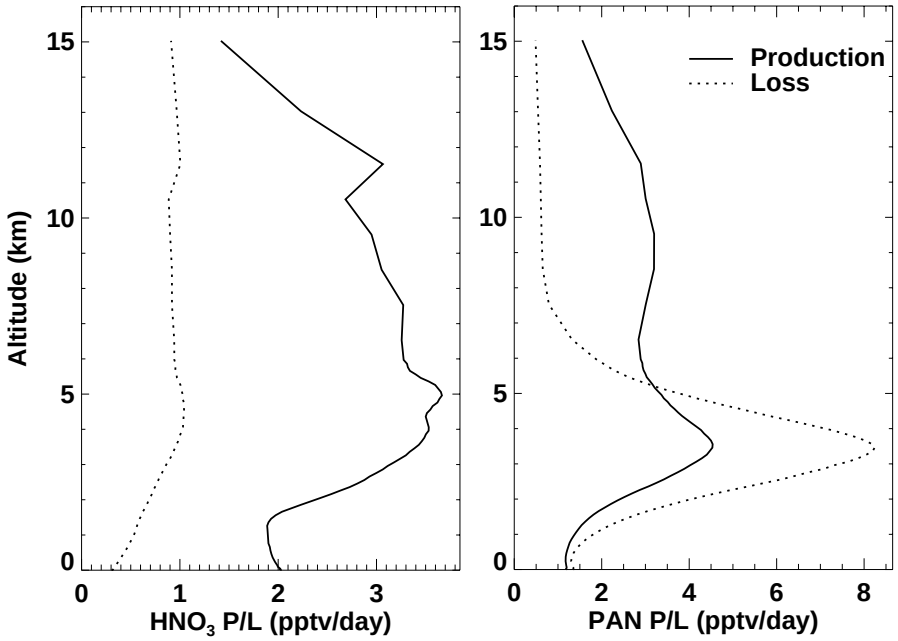

Figure 12 (Bottom)

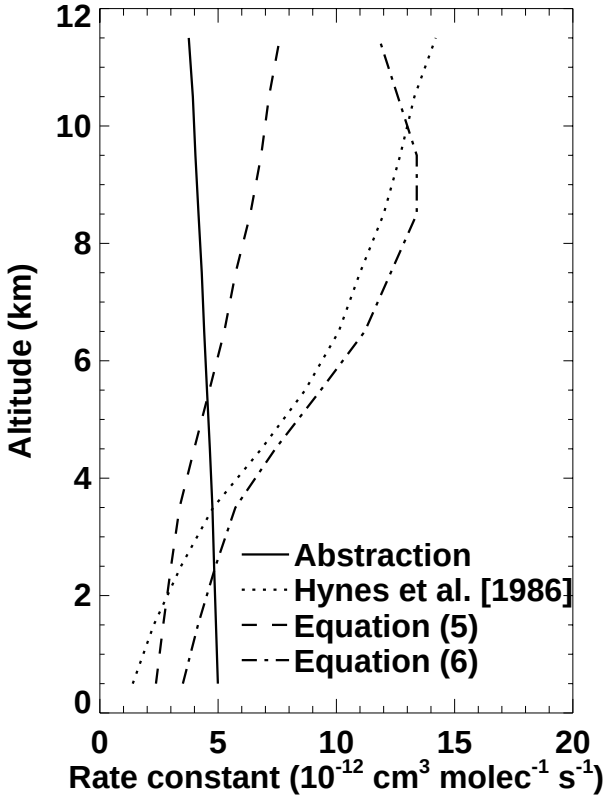

Figure 13 (Bottom)

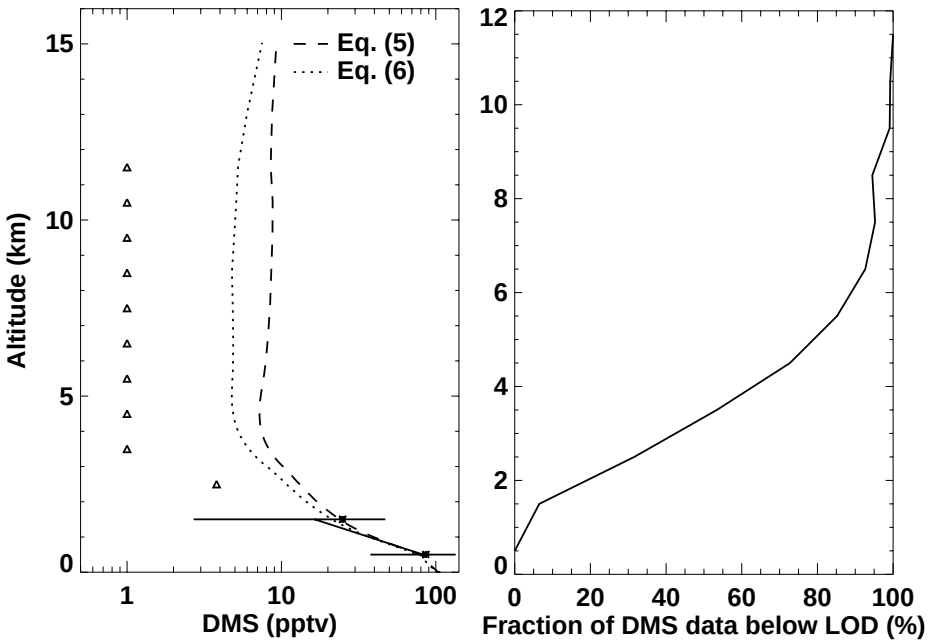

Figure 14 (Bottom)

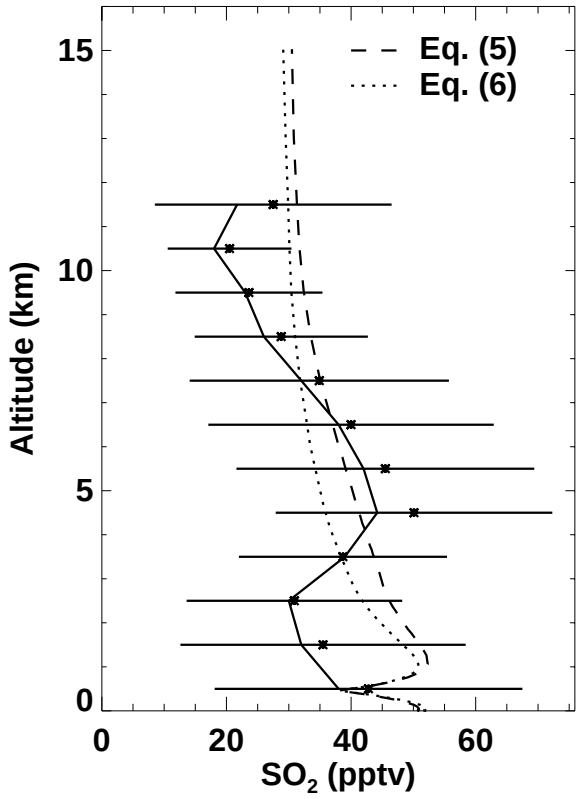

Figure 15 (Bottom)